

# Time-dependent delayed electron spectra: a direct measurement of total decay rate as a function of internal energy

F. Lépine, B. Climen, M.A. Lebeault, and C. Bordas<sup>a</sup>

Laboratoire de Spectrométrie Ionique et Moléculaire, UMR CNRS 5579, Université Lyon 1, 69622 Villeurbanne, France

Received 30 April 2009 / Received in final form 3 August 2009

Published online 7 November 2009 – © EDP Sciences, Società Italiana di Fisica, Springer-Verlag 2009

**Abstract.** We present a general method to measure internal energy dependant decay rate in the case of systems emitting thermal electrons. Our approach is based on the measurement of the time-dependent kinetic energy spectra of delayed electrons using time-resolved velocity map imaging spectrometry. We illustrate this method in the case of  $C_{60}$  molecules. Indeed electron spectra for  $C_{60}$  have been studied in great details in the past few years, allowing a complete analysis of the observed features. Moreover,  $C_{60}$  offers the opportunity to study competing decay mechanisms demonstrating that the technique may have broader applicability to other molecules. Using a model that includes all contributing decay channels relevant in our time delay range (namely delayed ionization and dissociation by  $C_2$  emission) we are able to derive quantitative information on the decay channels of the molecule. In the situation considered here, the time-dependent electron temperature extracted from the kinetic energy spectra is used to determine more precisely the rate constant for the dominant process, namely neutral  $C_2$  dissociation channel. In other words, the measurement of the cooling of an ensemble of  $C_{60}$  molecules as a function of time delay after heating provides a direct and quantitative access to its decay dynamics. This method may be used to map out the total rate for complex decay mechanisms.

**PACS.** 36.40.-c Atomic and molecular clusters – 33.60.+q Photoelectron spectra

## 1 Introduction

When a molecule is excited, its dynamical behavior depends on the details and nature of the excitation process as well as on the couplings between its various degrees of freedom. As a general rule, the more complex is the molecule, the less localized on a given degree of freedom is the excitation. This rule is even more appropriate in highly excited molecules where the density of accessible states becomes very high. This is a typical situation where Born-Oppenheimer approximation fails and vibronic couplings become of primary importance for the understanding of the time-dependent behavior of the system. When the excitation energy increases, new decay channels become accessible and compete among each other. This situation is fascinating from a fundamental point of view since accurate predictions on dynamics of very excited molecules are very demanding in terms of knowledge of potential energy surface of both ground and excited states. Therefore the theoretical description of such dynamics becomes untreatable on the microscopic quantum level, in a state-to-state approach. Yet, this complexity may result in a statistical behavior that can be more simply described within much simpler models [1] that do not necessarily take into account the details of the ongoing processes. The strength of the statistical hypothesis arises from the

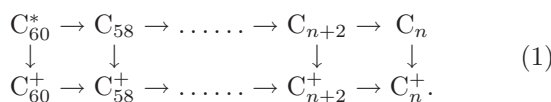
fact that the system undergoes a dynamics which does not depend on its detailed quantum structure or on the excitation process but on a few, very general, intrinsic properties: number of degrees of freedom, binding energies... From the experimental point of view, studying such processes is not simple due in particular to the existence of competing channels involving the emission of various types of particles (electron, photon, neutral/charged atoms or molecules) including neutrals, hardly detectable species. A priori, several detection techniques are necessary to perform a complete experiment. However, in many cases a detailed insight may be attained even if only one decay channel is monitored. In this contribution, we present a model example of this kind of process where the above experimental limitation may be largely overcome: namely the competition between delayed ionization and dissociation by emission of  $C_2$  of excited  $C_{60}$ . In this case, typical of a system exhibiting several competing decay mechanisms, the detailed measurement of the time-dependent delayed ionization spectra allows at the same time to follow the dominant neutral dissociation decay channel.

Delayed ionization of large molecules or clusters is a common process in highly excited systems. In the last 20 years, this phenomenon has been extensively studied, in particular in metal clusters, and its statistical nature has been demonstrated in many experiments [2]. In that

<sup>a</sup> e-mail: bordas@lasim.univ-lyon1.fr

context, fullerenes and more specifically  $C_{60}$ , have been the subject of numerous investigations [3–5]. Fullerene  $C_{60}$  represents a model system for studying the dynamics of ionization and energy couplings in complex systems. Its very high stability, combined with a large number of degrees of freedom allows preparing molecules in a very energetic state where several decay channels are open and contribute effectively in the decay of the molecule. Multiphoton nanosecond excitation of  $C_{60}$  followed by the fragmentation and ionization of the molecule was studied by time of flight spectrometry in a seminal work by Campbell et al. [5]. Multifragmentation, sequential dissociation, direct and delayed ionization were discussed in connection with the understanding of the bimodal structure of the time-of-flight spectrum measured. Subsequent studies have shown that the various decay channels also strongly depend on the time scale on which  $C_{60}$  is observed [6] and numerous works have been devoted to the disentanglement of the relative contribution and mechanisms responsible for the decay of  $C_{60}$ . The interpretation of delayed ionization in terms of statistical process has been a subject of large discussion. In early studies, most experimental data were based on time-of-flight measurements and analysis relied on single decay rate interpretation where the ion yield follows a simple exponential decay law [3–5]. However, the interpretation of experiments based on a direct connection between the lifetime of the molecule and the delayed ionization decay rate was not satisfactory owing to the broad internal energy distribution. Indeed, in order to be ionized during the typical accessible experimental observation time window (typically a few  $\mu s$  in a molecular beam experiment) the molecule needs to acquire a large amount of energy which requires a multiphoton process for a laser excitation in the visible or near-UV range. The complete description of the resulting internal energy distribution requires taking into account focal volume integration [7]. As a consequence a multiphoton excitation induces a broad internal energy distribution and therefore the dynamics observed cannot be described as a single decay rate (that would correspond to a single internal energy) process, which prevents a simple assumption.

More specifically in  $C_{60}$  delayed ionization is in competition with dissociation via sequential emission of  $C_2$  fragments. In all laser experiments so far only charged particles have been detected and the production of electrons or of a given ion  $C_n^+$  from photoexcited  $C_{60}$  results from the following decay chain:



Vertical arrows correspond to ionization steps with ejection of a single electron, horizontal arrows to dissociation steps with ejection of  $C_2$  units. Delayed ionization  $C_{60} \rightarrow C_{60}^+ + e^-$  and delayed dissociation  $C_{60} \rightarrow C_{58} + C_2$  are the dominant decay pathways for the  $C_{60}$  molecule on our accessible experimental timescale. Actually, the examination of Figure 1 displaying estimated decay rates of

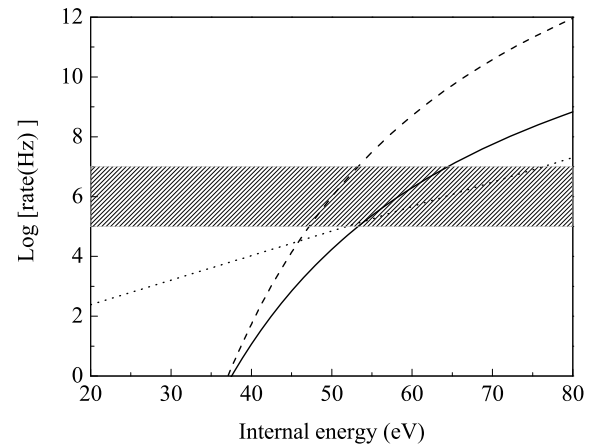


**Fig. 1.** Estimated emission rates for the major decay channels of  $C_{60}$ : thermionic emission (solid line), dissociation by emission of  $C_2$  (dashed line), blackbody emission (dotted line). Shaded area represents the accessible time range of interest in our experiment typically between 100 ns and 10  $\mu s$ . The dominant decay channel is clearly the dissociation channel competing essentially with thermionic emission. Blackbody radiation is neglected in the following.

$C_{60}$  allows a rather clear classification of dominant decay channels as a function of the internal energy of the fullerene molecule. The dissociation and blackbody radiation rates are estimated following reference [8] using the most recent parameter values of reference [9] while the thermionic emission rate is estimated according to reference [10]. The dissociation rate is by far the largest one in the range  $10^5$ – $10^7$  Hz, i.e. in the delay range below 10  $\mu s$ . Around 50 eV of internal energy, radiative cooling and thermionic emission have a comparable rate (around  $10^5$  Hz) but the decay dynamics is largely dominated by  $C_2$  emission which has a rate of about  $10^6$  Hz at this energy. At larger internal energies the dominant character of dissociation is even more pronounced. Actually radiative cooling starts to play a role at larger delays as it has been demonstrated in previous works [6,11] showing that the contribution of blackbody radiation becomes non negligible at delays slightly larger than 10  $\mu s$ . In the millisecond range radiative cooling is the dominant decay process. Therefore blackbody radiation will be neglected in the following, keeping in mind that it should be taken into account if measurement beyond 10  $\mu s$  were performed.

A significant breakthrough in the understanding of competing decay mechanisms in  $C_{60}$  occurred when Hansen and Echt [12] showed that the  $C_{60}^+$  ion yield as a function of the time delay after laser excitation could be described by a power law, and showed that the characteristic exponent of the power law is approximately the ratio between the ionization potential of  $C_{60}$  and the binding energy of  $C_2$  in  $C_{60}$  (denoted below as  $E_d$ ). These considerations allowed at that time the first accurate and relevant experimental determination of  $E_d$ . However, in order to obtain a complete understanding of the decay processes, it is necessary to know the rate constant for each channel, not only the binding energy. Generally the dissociation

rate is evaluated using an Arrhenius-like formula. Such a rate is determined by two constants, the binding energy  $E_b$  and the prefactor  $\omega_b$ . Note that strictly speaking the prefactor  $\omega_b$  is a slowly varying function of the energy and that it can be considered as a constant only over a limited time or energy range. Our method allows measuring the temperature of the excited species as a function of the time delay after excitation, in other words it provides an explicit relation between the total decay rate and the internal energy of the system without any assumption on the expression of the decay rate. The strength and the generality of our method rely in its capability of providing a direct access to the variation of the decay rate as a function of the excitation energy (or temperature). However, this does not prevent a further analysis based on additional assumptions allowing to extract relevant parameters from the measurements. Accordingly, as in previous works on  $C_{60}$  [6–13] the dissociation rate will be expressed using an Arrhenius-like formula, in order to derive the appropriate parameters.

In this article, we present experimental results on time-dependent kinetic energy spectra of electrons emitted upon delayed ionization of  $C_{60}$ . We show that measuring the time evolution of the electron spectrum allows extracting valuable information on the details of the decay mechanism through the precise measurement of temperature derived from these spectra as a function of the time delay after excitation. The time evolution of this temperature is of great interest since it provides a direct connection between the total decay rate of the  $C_{60}$  molecule and its internal temperature. In the present case we show that measuring the temperature as a function of the time delay allows measuring almost directly quantitative information on the major dissociation channel  $C_{60} \rightarrow C_{58} + C_2$ .

## 2 Theoretical framework and principle of rate measurements

A general description of the time-dependent kinetic energy spectrum in the case of competing decay mechanisms based on detailed balance theory has already been presented elsewhere [10]. In the following we summarize the main results obtained when it is applied to the case of  $C_{60}$ . Detailed balance theory allows the description of statistical emission of electrons [14], the so-called thermionic emission, from a neutral cluster or molecule when thermal equilibrium is assumed. The detailed balance theory relies mostly on the assumption of the reversibility of quantum processes. In this framework, the differential thermionic emission rate can be expressed as follows:

$$k_{el}(E, \varepsilon) = \frac{g^+}{g^0} 2 \frac{m}{\pi^2 \hbar^3} \sigma(\varepsilon) \varepsilon \times \exp\left(-\frac{\varepsilon}{k_B T_d^{el}(E)}\right) \exp\left(-\frac{\Phi}{k_B T_e^{el}(E)}\right). \quad (2)$$

In this expression,  $g^+$  and  $g^0$  correspond respectively to the degeneracy of the ion and the neutral molecule. Fol-

lowing the arguments presented in reference [15] the ratio  $g^+/g^0$  can be estimated around 10.  $E$  is the total energy of the system before ionization;  $\varepsilon$  is the electron kinetic energy;  $m$  and  $\sigma(\varepsilon)$  are respectively the electron mass and the energy-dependent cross-section for electron capture;  $\Phi$  is the electron binding energy (ionization potential). The microcanonical temperatures appearing in equation (2) are respectively the daughter temperature  $T_d^{el}(E)$  (microcanonical temperature of the system after emission of an electron) and the emission temperature  $T_e^{el}(E)$  that takes into account the finite heat bath correction [16]. These quantities depend explicitly on the internal energy  $E$ :  $T_d^{el}(E)$  is the internal temperature of a  $C_{60}$  molecule with an internal energy  $E_{daughter} = E - \Phi$ , and  $T_e^{el}(E)$  is approximately the temperature of a  $C_{60}$  molecule with an internal energy  $E_{emission} = E - \Phi/2$  [10,17]. If one defines respectively  $T_p(E)$  as the parent temperature (temperature of a  $C_{60}$  molecule of total internal energy  $E$ ) and  $C_v$  as the heat-capacity of  $C_{60}$  the daughter and emission temperature relevant to thermionic emission are respectively:

$$T_d^{el}(E) \approx T_p(E) - \frac{\Phi}{C_v}$$

and

$$T_e^{el}(E) \approx T_p(E) - \frac{\Phi}{2C_v}. \quad (2b)$$

In fact, rather than the classical constant value of the heat capacity of  $C_{60}$  ( $174 k_B$ ) we use in our calculations a more elaborate caloric curve found in the literature [18] (we use explicitly  $E(\text{eV}) = 14.17 + 0.01448(T - 1500)$ ).

Let us now consider an ensemble of fullerene molecules excited via a multiphoton process. The examination of the emission rates displayed in Figure 1 shows that an internal energy of about 50 eV is required in order to observe a decay on a typical timescale on the order of 1  $\mu\text{s}$ . This implies that an average number of about 15 photons at 355 nm is required in order to induce a decay process on typical experimental timescales. Owing to this relatively large number of photons and to the statistical character of the photon absorption, the internal energy distribution  $g(E)$  of the ensemble of  $C_{60}$  molecules contributing to the emission process is very broad. The time-dependent electron kinetic energy spectrum can be written as follows [10]:

$$P(\varepsilon, t) \propto \int g(E) k_{el}(E, \varepsilon) \exp(-K_{tot}(E)t) dE \quad (3)$$

where  $K_{tot}(E)$  refers to the total decay rate including the various possible decay channels. Considering the relevant timescales in the present study, and as it is visible in Figure 1, the total decay rate is mainly determined by the contributions of thermionic emission (rate  $K_{el}$ ) and of the dissociation channel leading to  $C_2$  emission [6] (rate  $K_{diss}$ ):

$$K_{tot}(E) = K_{diss}(E) + K_{el}(E). \quad (4)$$

The electron emission rate is obtained by integrating the differential rate introduced in equation (2).

The dissociation rate is chosen as an Arrhenius form:

$$K_{diss}(E) = \omega_d \exp\left(-\frac{E_d}{k_B T_e^{diss}(E)}\right) \quad (5)$$

where  $T_e^{diss}(E)$  is the emission temperature for the dissociative channel. Similarly to the emission temperature for delayed ionization it is defined as:

$$T_e^{diss}(E) \approx T_p(E) - \frac{E_d}{2C_v}. \quad (5b)$$

The dissociation rate varies extremely rapidly with the internal energy  $E$ . The internal energy distribution  $g(E)$  can be estimated by taking into account the geometrical properties of the excitation laser and molecular beams on one hand, and the Poissonian character of the multiphoton process on the other hand. As described in details in reference [7] this distribution may rather generally be represented as a power law of the energy  $g(E) \propto E^{-\gamma}$ . It follows that  $g(E)$  is a broad distribution that varies smoothly with  $E$  as compared to the other contributions of the integral in equation (3). On the other hand, at a given time delay  $t$ , the integral has significant values only around a given energy value  $E^*(t)$ , defined approximately by  $K_{tot}(E^*(t)) \approx 1/t$  [10]. The kinetic energy spectrum measured at a given time delay  $t$  corresponds therefore to electrons emitted from  $C_{60}$  molecules initially belonging to a narrow slice of the energy distribution centered around  $E^*(t)$ . Within a reasonable approximation we can assume that systems having an initial internal energy larger than  $E^*(t)$  have already decayed at time  $t$ , while the decay probability of systems with lower internal energy is almost negligible. As a consequence the electron kinetic energy spectrum at a given delay is essentially independent on the initial internal energy distribution (as soon as it is a broad distribution) and equation (3) can be approximated as follows:

$$K_{tot}(E^*(t)) \approx \frac{1}{t} \quad (6)$$

$$P(\varepsilon, t) \approx k(\varepsilon, E^*(t)) \exp(-K_{tot}(E^*(t))t). \quad (7)$$

The capture cross section in equation (2) is evaluated according to equation (20) in reference [10] taking into account the effect of the Coulomb potential and hard sphere contribution. Therefore the electron kinetic energy spectrum may be expressed as follows (see Eq. (21) in Ref. [10]):

$$P(\varepsilon, t) = C(t) (\varepsilon + V(R_0)) \exp\left(-\frac{\varepsilon}{k_B T_d^*(t)}\right) \quad (8)$$

where  $V(R_0)$  is the Coulomb potential at  $R_0$ , the hard sphere radius of  $C_{60}$  ( $V(R_0) \approx 4.1$  eV) and where the time-dependent daughter temperature is defined as follows:

$$T_d^*(t) = T_d(E^*(t)). \quad (9)$$

In most cases the ejected electron kinetic energy  $\varepsilon$  is smaller than 1 eV. Therefore according to equation (8) the kinetic energy spectrum is essentially an exponential function, with a small correction due to the hard sphere contribution to the cross section. As opposed to previous studies we do not neglect the term  $\varepsilon$  as compared to  $V(R_0)$  in the expression of the electron kinetic energy spectrum. However this introduces only a minor correction that shifts both the model and the fit by similar amounts without changing the comparison. Note that the cross section chosen assumes an electron sticking probability equal to 1 independently on its angular momentum.

In equation (8),  $C(t)$  is a time-dependent factor that determines simply the amplitude of the spectrum and decreases with time. The main parameter is the daughter temperature  $T_d^*(t)$ . This quantity may be fitted to the electron kinetic energy spectrum. Therefore its evolution as a function of time is accessible as soon as time-resolved electron spectra are recorded. Let us emphasize that the variation of the temperature with time does not correspond to a cooling process of a given  $C_{60}$  molecule but to the variation of the internal energy distribution of the ensemble of fullerene molecules. Due to the extremely fast variation of the emission rate as a function of internal energy, each time delay corresponds to a subset of fullerenes having a specific internal energy and therefore a well defined micro-canonical temperature. The experimental determination of  $P(\varepsilon, t)$  can be considered as a thermometric measurement for the fullerenes and gives access to the finite heat bath temperature. The time resolution allows the slicing of the, a priori unknown, large internal energy distribution. A well-defined temperature is determined for a given slice. If the caloric curve, connecting explicitly energy and temperature, is known, this measurement connects the time delay and the internal energy of the fullerenes. In other words the measurement of the daughter temperature  $T_d^*(t)$  as a function of time is a measurement of the decay rate as a function of the internal energy.

Let's point out that in the case where the total decay rate follows an Arrhenius-like expression  $K_{tot} = \omega_0 \exp(-E_0/k_B T_e)$  the approximate equation (6) may be linearized as follows:

$$(T)^{-1} \approx \frac{k_B}{E_0} \ln(t) + \frac{k_B}{E_0} (\ln(\omega_0)) \quad (10)$$

with  $T = T_d^*(t) + IP/C_v - E_0/2C_v$ . In other words, if one plots the inverse of the measured temperature (plus a finite bath correction) versus the logarithm of the time delay one obtains a quasi-linear curve with a slope equal to the inverse of the binding energy. The curve gives direct information on both the binding energy and prefactor  $\omega$ . Obviously, a perfect determination of these parameters would require measurements on large time scale since this determination depends on the logarithm of time. In any case it gives direct information on the rate. In the following, we illustrate this approach with measurements on  $C_{60}$  using time resolved imaging.

### 3 Experimental set-up

The experimental set-up used in this work combines a molecular beam, a time-of-flight mass spectrometer (TOFMS) and a time resolved velocity map imaging (VMIS) spectrometer. The  $C_{60}$  molecular beam is produced either by laser desorption of pure  $C_{60}$  powder embedded in a rod of organic material (matrix-assisted laser desorption), or by evaporation in a thermal oven. The first technique provides a very high flux of molecules but a high transverse velocity (about 1000 m/s) that prevents the detection of electrons at delays larger than a few  $\mu\text{s}$ . It is convenient for measurements at time delays less than 2  $\mu\text{s}$ . The oven technique is better for observations at larger delays. The velocity of fullerenes is reduced typically to 180 m/s and the  $C_{60}$  molecules leave the efficient detection region of the VMIS within about 10  $\mu\text{s}$ . It has been used for delays larger than 1  $\mu\text{s}$ . The extraction region of the photoelectron VMIS and the extraction region of the TOFMS are common and the set-up can be used either to obtain a mass spectrum or to detect electrons under strictly identical experimental conditions. The third harmonic of a Nd-Yag laser (10 Hz repetition rate, 355 nm, <10 ns pulse duration, max. 350 mJ/pulse) is focused onto the molecular beam using a 20 cm focal lens at the center of spectrometer to achieve multiphoton excitation.

The principle of charged particle imaging [19] introduced in the early 80's is extremely simple. A static electric field is used to accelerate the photoelectrons produced in the interaction region (crossing between the laser and the molecular beam) onto a position sensitive detector (PSD) that consists in a dual microchannel plate followed by a phosphor screen and a CCD camera. Our spectrometer is designed to minimize the effect of the initial geometrical dispersion of the emitting molecules following the principle of velocity-map imaging [20]. By summing electron impacts over many laser shots we obtain an image representing a map of the projection of the electrons velocity onto a plane perpendicular to the electric field used for the projection. If the laser polarization is chosen parallel to the detector, a standard inversion method [21] allows obtaining the distribution of velocity both in modulus and in direction. Angular-resolved photoelectron spectrum may subsequently be extracted from this distribution. Since the measurement of the electron velocity relies entirely on geometrical properties of the electron trajectories and since the time of flight of the electron is almost independent on its velocity, velocity-map imaging is intrinsically capable of time-resolution. By construction, the time of impact of the electron onto the PSD is precisely the time of emission of the electron from the excited species, augmented by the constant time delay corresponding to the time-of-flight of the electron. Therefore, by simply gating the voltage applied on the microchannel plates, one can switch the detection efficiency of the PSD allowing to select a given time window in which electrons are recorded. This given time window corresponds to a precise delay range after optical excitation of the fullerene molecules. Photoelectron images and delayed electron energy spectra in a well defined time window after the laser

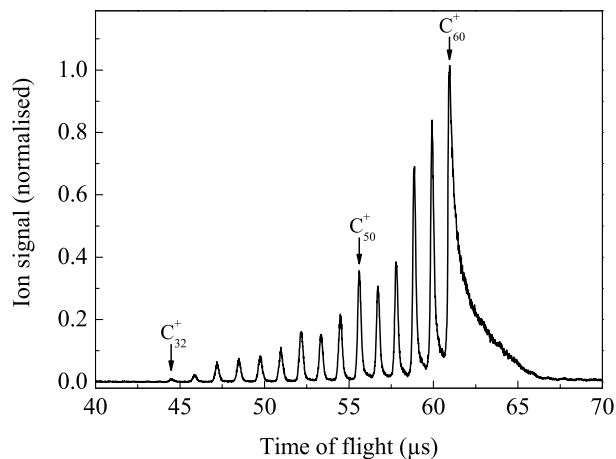


**Fig. 2.** Typical time of flight spectrum showing the fullerene fragmentation and the delayed ionization predominantly visible in the tail of the  $C_{60}^+$  peak. Ion fragments peaks correspond to electron emission possibly spanning the time range from 0 to 200 ns. This ensures that all electrons arriving onto the detector after a delay of about 200 ns arise directly from ionization of  $C_{60}$ . At shorter delays it is impossible to disentangle electrons ejected from various fragments. On the other hand, at larger delay, this mass spectrum ensures that only delayed ionization from  $C_{60}$  fullerenes contribute to the electron signal.

excitation can be measured. The best achievable time resolution of our system in its present configuration is about 60 ns, which is appropriate to the timescale of the observed phenomenon. Actually, in the present work we used integration windows between 100 ns and 1  $\mu\text{s}$ , depending on the intensity of the signal. In addition, the detection efficiency of velocity-map imaging is constant at threshold. This is absolutely required for studying precisely electron kinetic energy distributions that span the range from 0 to a few eV with a dominant contribution at low energy below 0.2 eV. Time resolved velocity-map imaging was used for the first time in the case of thermionic emission of  $C_{60}$  [22], and further extended to the study of other systems like small cluster anions [23]. Further details on the experimental technique are given elsewhere [24].

### 4 Results and discussion

A typical time of flight spectrum is presented in Figure 2. A strong  $C_{60}^+$  peak exhibiting a long tail extending over several microseconds is clearly visible. Ion fragments  $C_{60-2n}^+$  resulting from the sequential emission of  $n$   $C_2$  dimers and one electron emission are also clearly visible. For short delays (typically below 100 ns), no direct experimental argument allows us to assume that the detected electrons arise from the ionization of  $C_{60}$  as the first decay channel, or from the ionization of a smaller fragment  $C_{60-2n}$  after one or several  $C_2$  emission. However, under any experimental conditions, as exemplified in the typical spectrum of Figure 2, electrons detected after delays larger than about 200 ns may be entirely attributed to delayed ionization of  $C_{60}$  molecules. Indeed the

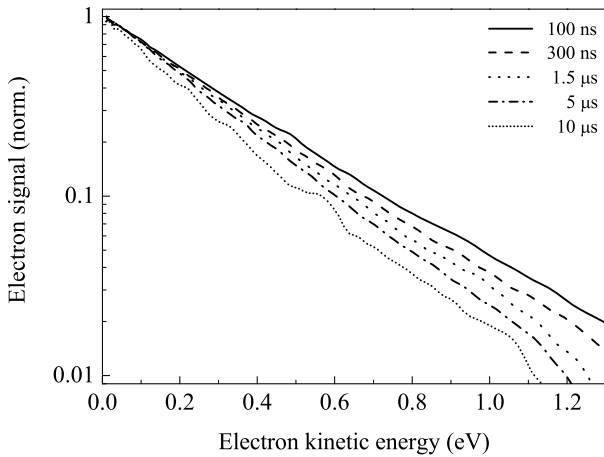


**Fig. 3.** Electron kinetic energy spectra recorded at various delays between 100 ns and 10  $\mu$ s after the laser excitation in an observation time window of 100 ns (for the shorter delays) or 1  $\mu$ s (for delays above 1.5  $\mu$ s). Spectra are displayed in logarithmic intensity scale in order to enhance the dominant exponential contribution.

$C_{60}^+$  ion peak exhibits substantial delayed ionization, while peaks of smaller fragments are significantly narrower and do not exceed about 200 ns in width, indicating that ionization of fragments with mass smaller than  $C_{60}$  occurs only in the early stage of the decay. Therefore all electrons detected at delays larger than 200 ns, as well as all corresponding spectra, may be entirely attributed to the single  $C_{60} \rightarrow C_{60}^+ + e^-$  ionization channel. At delays on the order of 100 ns or shorter it appears that a substantial part of electrons still come directly from  $C_{60}$ , however it is impossible to disentangle electrons ejected from various fragments.

Angle resolved electron velocity distributions have been recorded at several time delays from  $t = 100$  ns to  $t = 10$   $\mu$ s after the laser excitation. At shorter delays up to 2  $\mu$ s we use a narrow detection gate of about 100 ns, while at longer delays we enlarge the detection gate to 1  $\mu$ s in order to record a significant signal. More precisely the notation used throughout the paper is the following: for a given delay  $t_s$  up to 1  $\mu$ s we integrate during the time window  $t_s \pm 50$  ns, while for larger delays the integration time window is defined as  $t_s \pm 500$  ns. The observed photoelectron distribution is always isotropic and does not show any dependence as a function of the angle of emission with respect to the laser polarization. This is expected for a statistical emission process where the loss of coherence induced by the internal energy redistribution implies an isotropic emission. The corresponding kinetic energy spectrum is deduced from the angular integration of the image. Typical spectra are displayed in Figure 3 in logarithmic intensity scale in order to enhance the exponential shape of the kinetic energy distribution. Five typical spectra recorded with delays ranging from 100 ns to 10  $\mu$ s after the laser excitation are displayed.

In order to extract the microcanonical daughter temperature from the experimental data as a function of

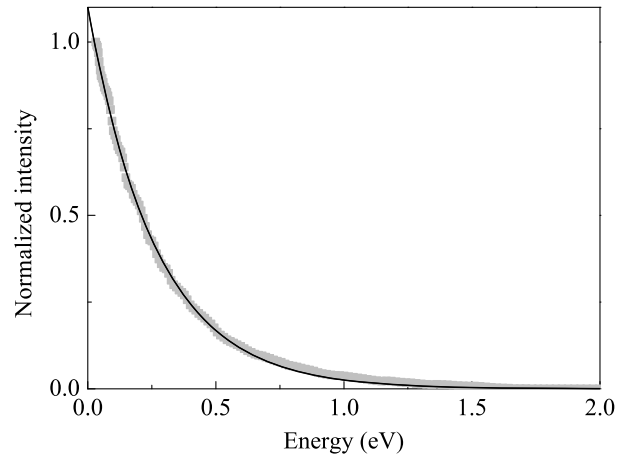


**Fig. 4.** Electron kinetic energy spectrum recorded 2  $\mu$ s after the laser excitation in an observation time window of 1  $\mu$ s (grey squares). The spectrum is fitted with a 2-free parameters procedure using a theoretical expression following equation (8) (black solid line). The fitting procedure allows us to determine a daughter temperature of  $2890 \pm 150$  K. In order to avoid slow photoelectron imaging effects the experimental spectrum is cut below 0.03 eV.

**Table 1.** Evolution of the fitted daughter temperature as a function of the time delay as presented in Figure 5. The temperature smoothly decreases from 3400 K at  $t = 100$  ns to 2500 K at  $t = 10$   $\mu$ s.

Time delay ( $\mu$ s)	Daughter temperature (K)	Estimated accuracy (K)
0.1	3360	100
0.3	3160	100
0.5	3070	100
0.8	3070	100
1	3030	100
1.2	3050	100
1.5	3000	100
2	2890	150
3	2860	150
4	2850	150
5	2800	150
6	2730	200
7	2680	200
8	2720	200
9	2590	250
10	2510	250

time delay we used a fitting procedure based on equation (8) with two free parameters: an arbitrary amplitude factor  $C(t)$ , and the daughter temperature  $T_d^*(t)$ . Figure 4 presents such a fitting procedure in the case of a delay  $t = 2$   $\mu$ s. We can notice the very good agreement between our experimental results and the theoretical profile of the spectrum. The deviation from the purely exponential shape is mainly due to the hard sphere component of the attachment cross section. Taking into account this contribution decreases the fitted temperature by about 200 K. For the present measurement we obtained  $T_d^*(2 \mu\text{s}) = 2890 \pm 150$  K. The fitted values are presented in Table 1,

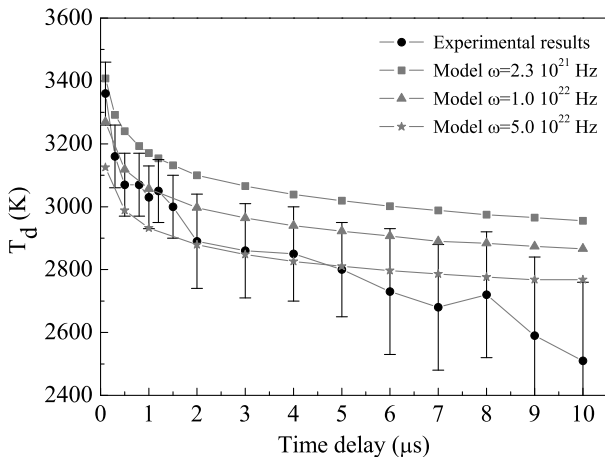


**Fig. 5.** Time evolution of the experimental daughter temperature (black line and circles, with error bars) compared to the temperature obtained with numerical simulations (gray lines and symbols) based on detailed balance theory including both thermionic emission and dissociation by emission of  $C_2$  fragments assuming a dissociation energy  $E_d = 10.6$  eV: gray squares  $\omega_d = 2.3 \times 10^{21}$  Hz; gray triangles  $\omega_d = 1.0 \times 10^{22}$  Hz; gray stars  $\omega_d = 5.0 \times 10^{22}$  Hz.

with corresponding error bars including the quality of the fitting procedure itself and the accuracy of the energy scale. More precisely the accuracy of the energy scale amounts for a systematic error in the range 1–2% while statistical uncertainties increase significantly at large delays where the electron signal is low. The evolution of the daughter temperature with time delay, major experimental results from this work, is displayed as full circles in Figure 5. The temperature smoothly decreases from about 3400 K at  $t = 100$  ns to about 2500 K at  $t = 10$   $\mu$ s. The smooth evolution is in agreement with the concept of a temperature driven by the total decay rate. Indeed the statistical theory predicts a fast variation of the decay rate with internal energy which means, in turn, a slow variation of the temperature within the range of accessible time delays. The uncertainty on the measurement increases with the time delay due to the decreasing of the electron signal intensity with time. Notice also that for larger delays the actual accuracy of our measurement may be affected due to the limitation of the performance of the VMIS when molecules leave the efficient zone of the spectrometer. Indeed the velocity of the molecules in the beam is around 180 m/s, which means that the excited molecules move by about 1 mm after 5  $\mu$ s. Given the actual design of our spectrometer this gives a maximum accessible time delay without sensible distortions of roughly 10  $\mu$ s.

The model presented in Section 2 allows us to derive expected temperatures as a function of the emission rates parameters. Measured temperatures are compared with those derived from the model in Figure 5. At each time delay we have numerically integrated equation (3) over internal energy and observation time window. The energy distribution is chosen as  $g(E) = E^{-\gamma}$  for  $E \leq E_c$  and as a Poisson distribution above the cut-off energy  $E_c$ .

The estimated values for  $\gamma$  and  $E_c$  were determined via a Monte-Carlo simulation of the time-of-flight spectrum measured under identical conditions as reported previously [25]. In agreement with works from other groups we found  $\gamma = 2.5$  and  $E_c = 110$  eV. Our calculation includes explicitly the contribution from thermionic emission (Eq. (2)) and from dissociation. The dissociation rate has been the subject of a large number of studies and discussion (see [9,26], and references therein). In this calculation we assumed a dissociation rate given by equation (5) using the most reliable values proposed by Concina et al. [9] who found  $E_d = 10.6$  eV, and  $\omega_d = 2.3 \times 10^{21}$  Hz. Each simulated spectrum is fitted with the same procedure that we used for the experimental data, allowing to derive an effective theoretical daughter temperature. The resulting temperatures are displayed as full squares in Figure 5. The overall smooth decrease of the temperature is well reproduced. The calculation leads to a variation of 300 K when the time delay varies from 500 ns to 10  $\mu$ s. Calculated values are close to the measured ones, though slightly above the error bars (experimental temperatures are typically 200 K lower than predicted values) which tends to show that  $\omega_d$  was slightly underestimated in [9].

From the literature, it is clear that the dissociation energy is more accurately determined than the prefactor owing to the various approaches leading to its derivation [9,12,13,26]. Therefore we consider the value from reference [9]  $E_d = 10.6$  eV as a fixed parameter and adjust the  $\omega_d$  prefactor. In order to illustrate the influence of the  $\omega_d$  prefactor two curves calculated respectively with  $\omega_d = 10^{22}$  Hz (triangles) and  $\omega_d = 5 \times 10^{22}$  Hz (stars) are plotted in Figure 5. Within our experimental accuracy we derive from our results  $\omega_d = 3 \pm 2 \times 10^{22}$  Hz.

Our present results give a somewhat higher value than previous estimations. This determination of  $\omega_d$  is however in reasonable agreement with other experimental determination [9,26] and theoretical calculations [8] predicting a high value of the dissociation energy and dissociation prefactor contrary to former results [27] in favor of a low binding energy and prefactor.

In principle the measurement performed here is appropriate to give an independent constraint on both the pre-factor and dissociation energy. This is of course one of the strength of the method consisting in connecting directly the total dissociation rate with the internal energy/temperature of the system. Nevertheless, a 2-free parameters fit gives very inaccurate values for both parameters due to the relatively large experimental error bars. This implies that, despite the almost direct determination of the total rate emission as a function of the temperature, we cannot determine separately  $E_d$  and  $\omega_d$  with a sufficient accuracy without any assumption on one of the constants. For instance a simple fit following the approximate procedure described by equation (10) is presented in Figure 6. A fitting procedure restricted to the range of delays not larger than 5  $\mu$ s assuming a total rate approximated by the dissociation rate, and with no assumption on both parameters, leads to  $E_d \approx 5.90$  eV and

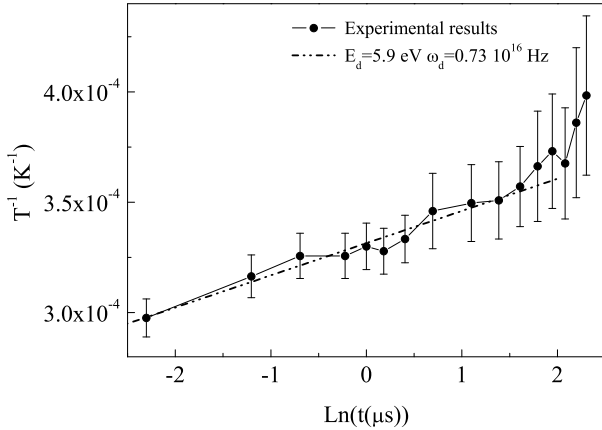


**Fig. 6.** Inverse of the temperature plotted as a function of the natural logarithm of time delay (experimental results: black circles with error bars). In the simplest approximation  $T^{-1}$  is a linear function of  $\text{Ln}(t)$  such as described in equation (10). The dashed-dotted line is a linear fit (restricted to experimental delays not larger than  $5 \mu\text{s}$ ) on equation (10) leading to  $E_d = 5.90 \text{ eV}$  and  $\omega_d = 0.73 \times 10^{16} \text{ Hz}$ . Both values are not physically significant and a fit without any assumption on  $E_d$  leads to irrelevant results.

$\omega_d \approx 0.73 \times 10^{16} \text{ Hz}$ . Although rather satisfactory (see Fig. 6, standard deviation  $= 3.64 \times 10^{-6}$ ), this fit leads to values without any physical signification, mainly due to the strong correlation between both parameters.

This discrepancy, mostly noticeable at larger delays in the case of the more refined model presented in Figure 5 where  $E_d$  is a fixed parameter, may arise from two very different origins. The first one is the poorer quality of experimental measurements at delays exceeding a few  $\mu\text{s}$ . This limitation could be raised by improving the method in order to have access to larger delays. In any case, it is clear experimental evidence that measured temperatures are found below the expected values in this range of delays and, assuming the reliability of our experimental results points to another origin in this discrepancy. Indeed, the Arrhenius relation giving the dissociation rate (Eq. (5)) with a constant frequency factor  $\omega$  is only approximate and, while the dissociation energy is an absolute quantity with a precise meaning, the prefactor  $\omega$  is a slowly varying function of the energy (or temperature) and a unique determination may not be absolute. Therefore, the deviation observed between our measurements and the prediction of our model based on the more reliable experimental values of  $E_d$  and  $\omega_d$  could arise from a deviation from the standard Arrhenius relation. More refined descriptions of the dissociation rate, such as those introduced in [15], are required in order to analyze further this aspect. The disagreement between the complete model and the experimental results is however relatively small. In the analysis we assumed that the electron emission rate is given by Weisskopf theory (Eq. (2)) and an Arrhenius like expression for the dissociation rate has been used (Eq. (5)). Both agree with previous experimental and theoretical estimations but our results seem to show

that the dissociation rate was slightly underestimated. Of course an accurate determination of the rate requires a very accurate determination of the temperature. In order to achieve  $\delta \ln(K_d(E)) < 1$  (determination of the rate by one order of magnitude), the required accuracy on the temperature is typically  $\delta T_d^*(t) < 100 \text{ K}$  which is precisely our experimental precision. A better determination of the rate could then be possible if one reaches the limit of resolution of the velocity-map imaging spectrometer which is typically 1%. Note also that as long as the experimental observations are performed at delays shorter than  $10 \mu\text{s}$  the influence of blackbody radiation is negligible within our experimental accuracy and radiative cooling cannot be invoked in order to account for the observed discrepancy.

Before concluding this discussion let us comment briefly the various approximations used in our analysis and the effective limitations to a precise determination of the emission rate. One of the approximations proposed in our model consists in neglecting the width of the time-window. However since the rate varies strongly with the temperature, the variation induced by this approximation is very small. Combining equations (5) and (6) allows expressing the error  $\Delta E$  on the internal energy induced by the uncertainty  $\Delta t$  on the time delay as:

$$\Delta E = \frac{\Delta t}{t} \frac{k_B C_v T_{ed}^2}{E_d}. \quad (11)$$

For instance,  $t = 1.0 \pm 0.5 \mu\text{s}$  leads to  $E = 45 \pm 0.5 \text{ eV}$ . This means that the uncertainty on the temperature due to the finite width of the integrating time window is merely 1%, i.e. comparable to the experimental accuracy of the energy measurement in velocity map imaging. As a result, averaging the temperature over the time window induces a variation of the measured temperature within the experimental error bars and the influence of the width of the time window can be neglected in the analysis. In the above determination of  $\omega_d$  we also assumed that the internal energy distribution is very broad as compared to the rapidly varying rate constant. The correction to the estimated temperature due to the finite width of the internal energy is connected to the exponent  $\gamma$  introduced above. It is almost negligible and at most on the order of 1 K.

Finally, let's recall that measurements performed on slow electrons are difficult. Besides the experimental difficulty due to the extreme sensitivity to any external perturbation (this is in principle taken into account by a careful design of the set-up) slow electrons are also extremely sensitive to intrinsic properties of the system and the interaction between the slow escaping electron and the residual  $\text{C}_{60}^+$  ion has a (weak) signature in the image. Based on previous experiments on slow photoelectron imaging, we know that inversion procedure would eventually fail to reconstruct the velocity distribution of electron with very low kinetic energy. Such effect is responsible for alteration of the spectrum at threshold [28] and in every case experimental spectra have been cut below  $0.03 \text{ eV}$  in order to remove the additional zero-energy peak arising from the Coulomb interaction between the ion and the

escaping electron. Moreover, an accurate determination of the temperature from the analysis of our experimental electron kinetic energy spectra would in principle require a very accurate determination of the attachment cross section. Indeed, this cross section directly influences the shape of the electron spectrum (see Eq. (2)) and therefore has an influence on the fitted temperature. As it can be noticed on the experimental spectrum presented in Figures 3 and 4, the small difference in the shape of the experimental and calculated KES is sufficient to induce an error of a few percent on the determined temperature. A more refined model of the electron attachment cross section could help in a very accurate determination of the dissociation rate. However, at the present level of experimental accuracy and of model refinement we are not able to determine if the weak difference observed arises from an experimental limitation or from an inaccurate theoretical shape of the KES.

## 5 Conclusion

We have performed time resolved measurement of the kinetic energy spectrum of delayed electron emission. These measurements allowed us to determine an accurate daughter temperature of the fullerene ion thanks to the fast variation of the decay rate as a function of internal energy/temperature. Besides the (approximate) direct measurement of the total emission rate as a function of the excitation of the fullerene, a single series of measurements spanning a broad time-window (from 100 ns to 10  $\mu$ s) is found to agree with previous results obtained generally for single values of the delay after excitation. In addition, we observed a small difference between the predictions of our model based on detailed balance theory and on the known values of the dissociation rate parameters, and our experimental results. Our experimental results tend to indicate a higher value for the dissociation rate constant as a function of temperature, and an increasing discrepancy between experiment and modeling as the time delay increase. Assuming the most reliable dissociation energy value in the literature ( $E_d = 10.6$  eV) we re-estimate the dissociation rate prefactor  $\omega_d = 3 \pm 2 \cdot 10^{22}$  Hz.

The assumption of the rate driven temperature is in principle able to give further information on the decay rate but is however limited by the finite precision on the experimental temperatures even though it is relatively small (few %) and by the limited timescale experimentally explored. In our technique, at a given time delay only a narrow internal energy range contributes to the kinetic energy spectrum. Time-dependent kinetic energy spectrum can be seen as a “slicing” of the internal energy distribution and each slice can be studied via the shape of the electron spectrum allowing us to extract information on the intrinsic dynamics of the system. This technique can be useful to study and disentangle the different decay mechanisms of highly excited molecules or clusters and could be applied to many other complex molecular systems including biomolecules.

We gratefully acknowledge Klavs Hansen for fruitful discussions and comments on this work.

## References

1. K. Hansen, *Philos. Mag. B* **79**, 1413 (1999)
2. E.E.B. Campbell, R.D. Levine, *Annu. Rev. Phys. Chem.* **51**, 65 (2000)
3. P. Wurz, K.R. Lykke, *J. Phys. Chem.* **96**, 10129 (1992)
4. P. Sandler, C. Lifshitz, C.E. Klots, *Chem. Phys. Lett.* **200**, 445 (1992)
5. E.E.B. Campbell, G. Ulmer, I.V. Hertel, *Phys. Rev. Lett.* **67**, 1986 (1991)
6. F. Rohmund, M. Heden, A.V. Bulgakov, E.E.B. Campbell, *J. Chem. Phys.* **115**, 3068 (2001)
7. K. Mehlig, K. Hansen, M. Heden, A. Lassesson, A.V. Bulgakov, E.E.B. Campbell, *J. Chem. Phys.* **120**, 4281 (2004)
8. C. Lifshitz, *Int. J. Mass. Spectrom.* **198**, 1 (2000)
9. B. Concina, S. Tomita, J.U. Andersen, P. Hvelplund, *Eur. Phys. J. D* **34**, 191 (2005)
10. F. Lépine, C. Bordas, *Phys. Rev. A* **69**, 053201 (2004)
11. J.U. Andersen, C. Brink, P. Hvelplund, M.O. Larsson, B. Bech Nielsen, H. Shen, *Phys. Rev. Lett.* **77**, 3991 (1996)
12. K. Hansen, O. Echt, *Phys. Rev. Lett.* **78**, 2337 (1997)
13. S. Tomita, J.U. Andersen, C. Gottrup, P. Hvelplund, U.V. Pedersen, *Phys. Rev. Lett.* **87**, 073401 (2001)
14. V. Weisskopf, *Phys. Rev.* **52**, 295 (1937)
15. K. Hansen, E.E.B. Campbell, O. Echt, *Int. J. Mass Spectrom.* **252**, 79 (2006)
16. C.E. Klots, *Z. Phys. D* **5**, 83 (1987)
17. J.U. Andersen, E. Bonderup, K. Hansen, *J. Chem. Phys.* **114**, 6518 (2001)
18. B. Tsipinyuk, A. Budrevich, M. Grinberg, E. Kolodney, *J. Chem. Phys.* **106**, 2449 (1997)
19. *Imaging in Molecular Dynamics Technology and Applications*, edited by B.J. Whitaker (Cambridge University Press, 2003)
20. A.T.J.B. Eppink, D.H. Parker, *Rev. Sci. Instrum.* **68**, 3477 (1997)
21. C. Bordas, F. Paulig, H. Helm, D.L. Huestis, *Rev. Sci. Instrum.* **67**, 2257 (1996)
22. F. Lépine, B. Climen, F. Pagliarulo, B. Baguenard, M.A. Lebeault, C. Bordas, M. Hedén, *Eur. Phys. J. D* **24**, 393 (2003)
23. J.B. Wills, F. Pagliarulo, B. Baguenard, F. Lépine, C. Bordas, *Chem. Phys. Lett.* **390**, 145 (2004)
24. B. Baguenard, J.B. Wills, F. Pagliarulo, F. Lépine, B. Climen, M. Barbaire, C. Clavier, M.A. Lebeault, C. Bordas, *Rev. Sci. Instrum.* **75**, 324 (2004)
25. B. Climen, B. Concina, M.A. Lebeault, F. Lépine, B. Baguenard, C. Bordas, *Chem. Phys. Lett.* **437**, 17 (2007)
26. S. Tomita, J.U. Andersen, K. Hansen, P. Hvelplund, *Chem. Phys. Lett.* **382**, 120 (2003)
27. E. Kolodney, B. Tsipinyuk, A. Budrevich, *J. Chem. Phys.* **102**, 9263 (1995)
28. C. Bordas, *Phys. Rev. A* **58**, 400 (1998)